ACS MATERIALS LETTERS

www.acsmaterialsletters.org

LETTER

Fabrication and Photoluminescence Studies of Tin-Vacancy Centers in Chemical Vapor Deposition Diamond

Rani Mary Joy,* Miquel Cherta Garrido, Omar J. Y. Harb, Hendrik Jeuris, Rozita Rouzbahani, Jan D'Haen, Stephane Clemmen, Dries Van Thourhout, Danny E. P. Vanpoucke, Paulius Pobedinskas, and Ken Haenen*

Cite This: https://doi.org/10.1021/acsmaterialslett.5c01218

Read Online

ACCESS | Metrics & More | Article Recommendations | Supporting Information

ABSTRACT: **Group IV color centers in diamond are promising single-photon emitters for quantum information processing and networking. Among them, the tin-vacancy (SnV) center stands out due to its long spin coherence times at cryogenic temperatures above 1 K. While SnV centers have been realized using various fabrication routes, their in situ formation via microwave plasma-enhanced chemical vapor deposition (MW PE CVD) remains relatively unexplored. In this study, SnV centers, identified by a zero-phonon line (ZPL) near 620 nm, were synthesized in nanocrystalline diamond and free-standing microcrystalline diamond using tin oxide (SnO_2) as a dopant source at substrate temperatures of 750°C and 850°C. Photoluminescence measurements reveal that lowering the substrate temperature enhances both the ZPL intensity and spatial uniformity of SnV centers. These results highlight substrate temperature as a key parameter for controlling SnV incorporation during MW PE CVD growth and provide insights into optimizing fabrication strategies for diamond-based quantum technologies.**

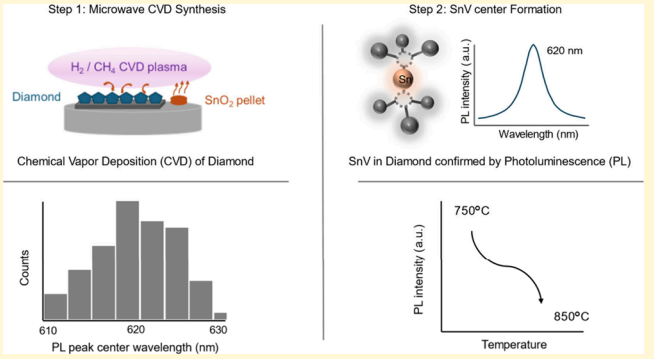

Advancements in photonics have highlighted the suitability of diamond as a material platform for quantum information processing applications.[1−3] These all-optically controlled diamond systems are primarily based on the nitrogen-vacancy (NV) center due to its extended spin coherence times at room temperature.[4] However, enhancing its optical performance with nanostructures and stability remains a challenge, given its sensitivity to the diamond surface conditions.[5,6] Promising alternatives are the Group IV color centers in diamond that have a split vacancy configuration with an interstitial Group IV atom. They exhibit inversion symmetry and are less affected by first-order electric fluctuations with minimal spectral diffusion, making them potential quantum network nodes in an integrated photonics platform.[7,8] The widely reported Group IV color centers are the silicon-vacancy (SiV) and germanium-vacancy (GeV) centers in diamond.[9] Compared to the SiV and GeV, the tin-vacancy (SnV) center in diamond, with a zero phonon line (ZPL) at ≈620 nm, has a long spin coherence time in the millisecond range already at temperatures below 2 K,[10] not requiring further cumbersome cooling to the mK range.[2]

The state-of-the-art fabrication strategies for the SnV center in diamond are the high-pressure high temperature (HPHT), ion implantation-annealing, and shallow ion implantation-chemical vapor deposition (CVD) overgrowth and detonation processes.[11−15] However, these techniques have multiple steps or require further processing. In contrast, the microwave plasma-enhanced chemical vapor deposition (MW PE CVD) technique in the presence of a Sn precursor, facilitates a scalable in situ creation of SnV centers in diamond in a single process step. Currently, only a few studies have reported SnV in CVD diamond.[10,16] However, the effect of CVD process conditions on SnV photoluminescence (PL) properties is currently lacking and forms the primary motivation of this study. While low-strain single crystal diamond is generally

Received: September 2, 2025
Revised: November 13, 2025
Accepted: November 18, 2025

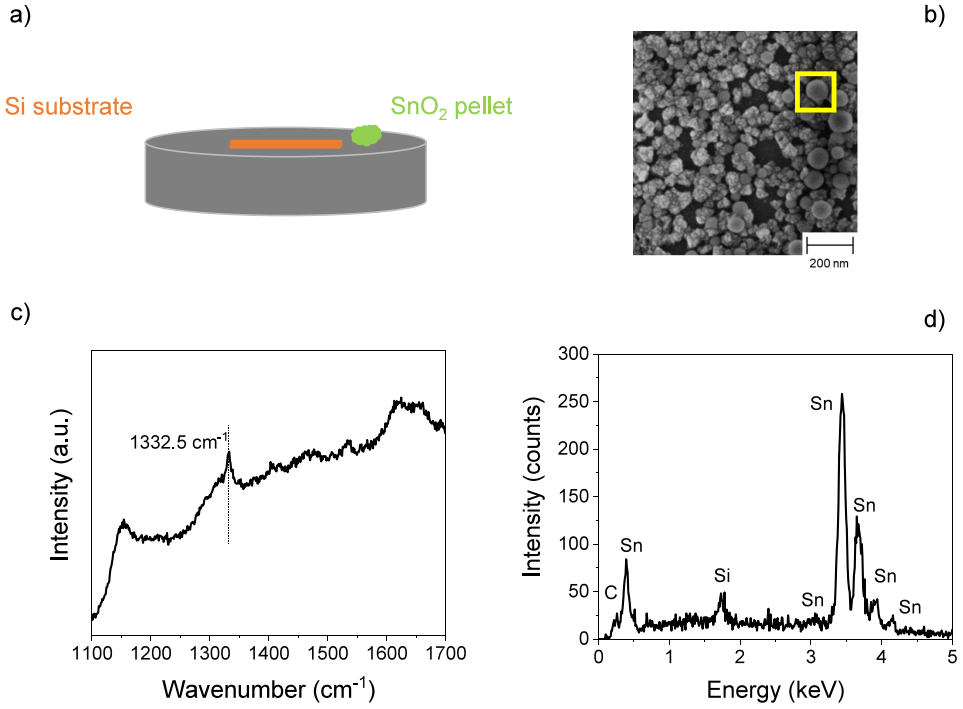

Figure 1. (a) Schematic illustration of NCD growth on silicon substrate in the presence of SnO_2 pellet, (b) SEM image of the resulting NCD with randomly oriented grains and spherical features; the yellow square indicates the region selected for elemental analysis, (c) Raman spectrum recorded from a representative NCD region of the sample, and (d) EDX spectrum acquired from the area highlighted in (b) confirming the presence of tin.

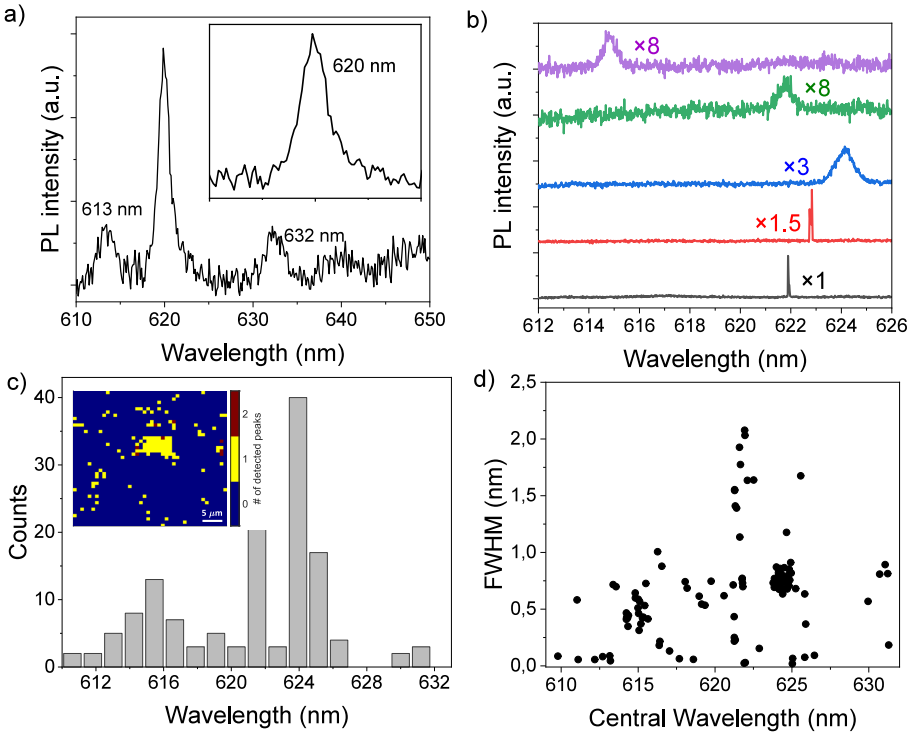

Figure 2. Representative PL spectra of NCD on Si substrate recorded at (a) 300 K and 7.5 K, (b) a selection of the most representative spectra found in a scanned area of 40 μm × 40 μm; the spectra are vertically offset and multiplied by the indicated factor, (c) central wavelength histogram of detected spectral peaks at 7.5 K with the corresponding PL map (inset), and (d) distribution of the central wavelength and the fwhm of detected peaks from the same PL map.

preferred for color center research, polycrystalline diamond provides a cost-effective and adequate environment for color center process optimization in CVD diamond.[17,18]

Here, we report the formation of SnV centers in CVD polycrystalline diamond grown at different substrate temperatures, overcoming solid dopant-related limitations using a

https://doi.org/10.1021/acsmaterialslett.5c01218
ACS Materials Lett. XXXX, XXX, XXX−XXX

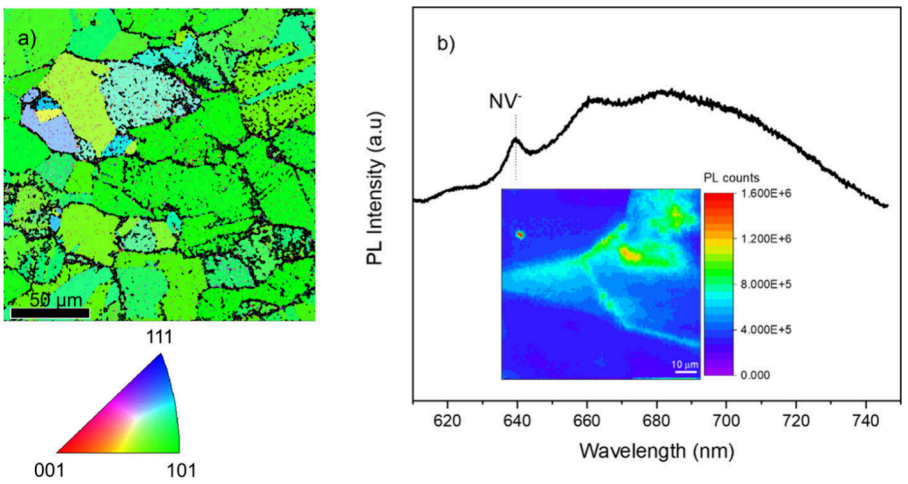

Figure 3. MCD substrate characterization. (a) Representative inverse pole figure with crystal orientation along the *z*-axis; the color code corresponding to the crystal orientation is given in the triangle, and (b) typical room temperature PL characterization results. The MCD substrate shows a predominant (110) grain orientation with the negatively charged NV center as the prominent optically active defect.

modified substrate holder. PL characteristics of SnV centers in nanocrystalline diamond (NCD) and free-standing (110)-oriented microcrystalline diamond (MCD) fabricated with tin oxide (SnO_2) as the solid dopant source are presented. Our PL results confirm the formation of SnV centers in diamond, as evidenced by the ZPL at ≈620 nm, with spatial nonuniformity in all samples. Additionally, a range of PL peaks is observed that could be attributed to the fabrication-induced strain. This correlation is further supported by theoretical studies under hydrostatic conditions, thereby providing a better understanding of the PL spectra observed in this study.

Two types of substrates were used − Si (100) and free-standing polished MCD discs. Substrate details and their preparation can be found in the Supporting Information (SI). First, diamond growth was carried out on Si substrates in the ASTeX 6500 MW PE CVD system using a process gas mixture of 1% methane in hydrogen, total gas flow of 500 sccm, working pressure and MW power of 25 Torr and 2000 W, respectively. The substrate and pellet of SnO_2 (Kurt J. Lesker 99.9% purity), placed 5 mm from each other (schematic in Figure 1(a)), are simultaneously exposed to the diamond growth conditions for a duration of 1 h.

Figures 1(b) and 1(c) show a representative scanning electron microscopy (SEM) image and Raman spectrum of the NCD sample. SEM reveals randomly oriented grains accompanied by spherical features, while the characteristic Raman peak at 1332.5 cm^{-1} confirms diamond formation under these CVD conditions. Energy-dispersive X-ray (EDX) analysis of these spherical features confirms that their composition is primarily Sn (Figure 1(d)). A study has shown that hydrogen-rich plasma reduces SnO_2 to elemental Sn,[19] hence sublimation and plasma etching of Sn on exposure to diamond CVD conditions can be expected. We estimate a growth temperature of (650 ± 20)°C, (measured using a dual wavelength Williamson Pro92 pyrometer), well above the melting point of ≈231 °C.[10] During diamond growth, we observe sparks on the dopant pellet surface that are likely due to Sn ejection,[20] leading to Sn deposits on the substrate. Such deposits partially inhibit diamond growth; thus, a continuous and fully closed diamond film is not observed in this sample, indicating a significant process challenge when using tin oxide as the dopant source. Experiments were carried out to study the effect of the proximity of the dopant source and substrate on the subsequent diamond coverage on the substrate. A 1 mm lateral separation between the pellet and substrate resulted in an almost complete Sn coverage on the Si surface. In general, as the lateral separation increased, the Sn coverage decreased. At 5 mm separation, we estimate diamond growth of at least 30% of the substrate (analyzed with SEM), and the sample was chosen for further characterization.

Room temperature PL analysis confirms SnV formation in NCD, as evidenced by the 620 nm PL peak (Figure 2(a)). Additional peaks at 613 and 631 nm are also observed, which motivated cryogenic PL characterization at 7.5 K. Figures 2(b) and 2(c) show examples of the PL spectra, and the corresponding histogram of the center wavelength distribution observed in NCD, obtained from a 40 μm × 40 μm mapping area, respectively. It is evident that the most frequent peak is around 624 nm. The vast majority of the peaks at 624 nm observed in the mapped area are localized in a region of around 50 μm^2, clearly indicating spatial nonuniformity of SnV formation in the sample (Figure 2(c) inset shows the PL map). A peak shift of 4 nm, relative to the unstrained SnV ZPL,[11] along with a broad and uniform line width of approximately 0.6 nm, is observed for the 624 nm spectral line. Our previous study of the GeV center in NCD films indicates that PL peak shifts are strain-induced,[21] while ZPL broadening and fine structure masking are associated with the diamond lattice dislocations.[22] Based on the above, we attribute the ZPL shift and broadening manifested in the 624 nm spectral line to the effects of strain and the polycrystalline nature of the NCD sample. The second most common wavelength was at 622 nm, with the line width ranging from below 0.1 nm to above 2 nm (Figure 2(d)). The majority of the 622 nm lines are qualitatively similar to the 624 nm peak. Although rarer, narrow spectral lines around 622 nm are also detected in this sample. These features, similar to the literature,[10] are indicative of single centers or few ensemble clusters. Furthermore, the 615 nm line is comparable to the 624 nm feature, but it is not localized within a specific sample area.

A majority of the spectral lines are either blue or red-shifted (Figure 2(d)) from the SnV ZPL. Stress-related ZPL shifts have been reported for SiV, GeV, and SnV in diamond.[10,21,23] To further investigate stress, Raman spectroscopy was

https://doi.org/10.1021/acsmaterialslett.5c01218
ACS Materials Lett. XXXX, XXX, XXX−XXX

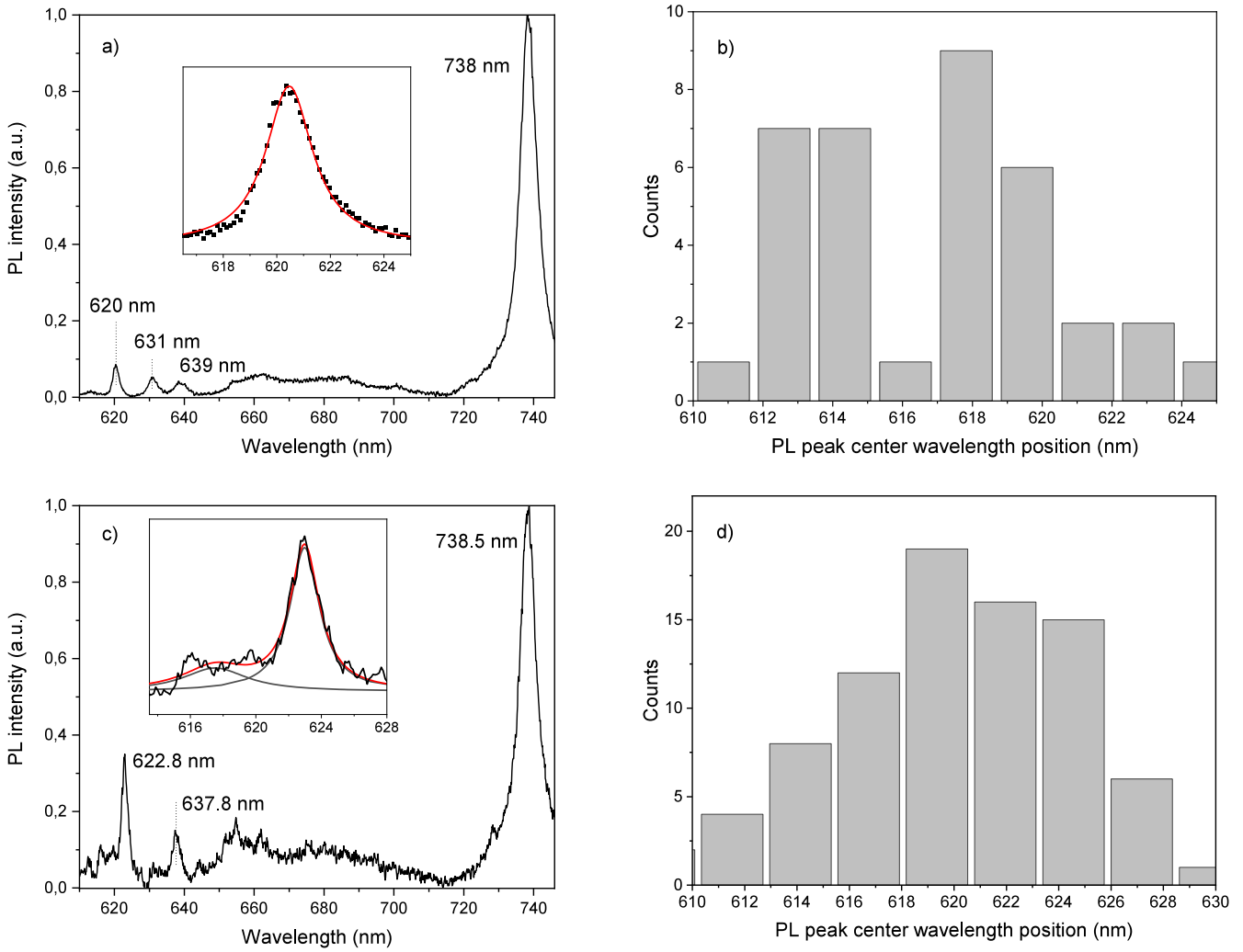

Figure 4. Room temperature PL spectrum and the corresponding PL peak center position distribution in the MCD samples S850 (a,b) and S750 (c,d), respectively.

performed on the sample, but significant shifts in the diamond Raman peak were not observed. Nevertheless, based on the reported SiV ZPL variation in nanodiamonds,[23] we propose nonuniform strain to be present in the local environment of the SnV in NCD at different locations of the sample.

Attempts made to increase NCD coverage on the Si substrate by placing it at 3 mm elevation, in addition to the lateral separation, resulted in a continuous diamond film with well-faceted NCD morphology and Sn deposits (SI Figures S1 and S2). Relatively few SnV centers were identified, and we attribute it to the higher substrate temperature of (750 ± 20)°C resulting from the sample's placement further into the CVD plasma. To further investigate the effect of substrate temperature on SnV formation, CVD diamond process in the presence of SnO_2 was also carried out on MCD substrates (Figure 3). First, the MCD substrate underwent electron backscatter diffraction (EBSD) and room temperature PL characterization. Results show that the MCD substrate has a predominant (110) grain orientation, while NV centers are the dominant optically active defects in the MCD substrate, and luminescent grain boundaries appear as bright regions in the PL mapping.

Diamond growth was carried out using the same process gas ratio of 1% methane in hydrogen as used for the NCD sample, simultaneously exposing the MCD substrate and SnO_2 pellet to the diamond CVD conditions for a duration of 3 h. The substrate Sn coverage was alleviated at 3 mm elevation and a 5 mm lateral separation from the dopant source. But placing the MCD substrate further into the plasma results in a higher substrate temperature. To maintain the substrate temperature at 750 and 850 °C, MW power of 3000 and 3500 W with working pressure of 45 Torr were used, respectively, and are henceforth named S750 and S850 in this manuscript. Sn deposits were observed on the sample surface, and after the CVD diamond process, the samples were wet-chemically etched (procedure described in SI) and inspected with an optical microscope (Zeiss Axiovert 40 MAT) to locate regions of overgrown diamond, followed by room-temperature PL characterization. Trapped Sn deposits within the overgrown diamond layer hamper an accurate thickness determination of the overgrown diamond film, and we estimate a film thickness of about (5 ± 2) μm from the depth scans carried out on the sample using the confocal PL measurement setup.

Figure 4(a) shows a typical room temperature PL spectrum of the S850 sample. The most intense peak at ≈ 738 nm corresponds to the well-known ZPL of SiV centers in diamond.[24] Si is an unintentional dopant in this process, with its origins speculated to be residual or quartz parts of the

https://doi.org/10.1021/acsmaterialslett.5c01218
ACS Materials Lett. XXXX, XXX, XXX−XXX

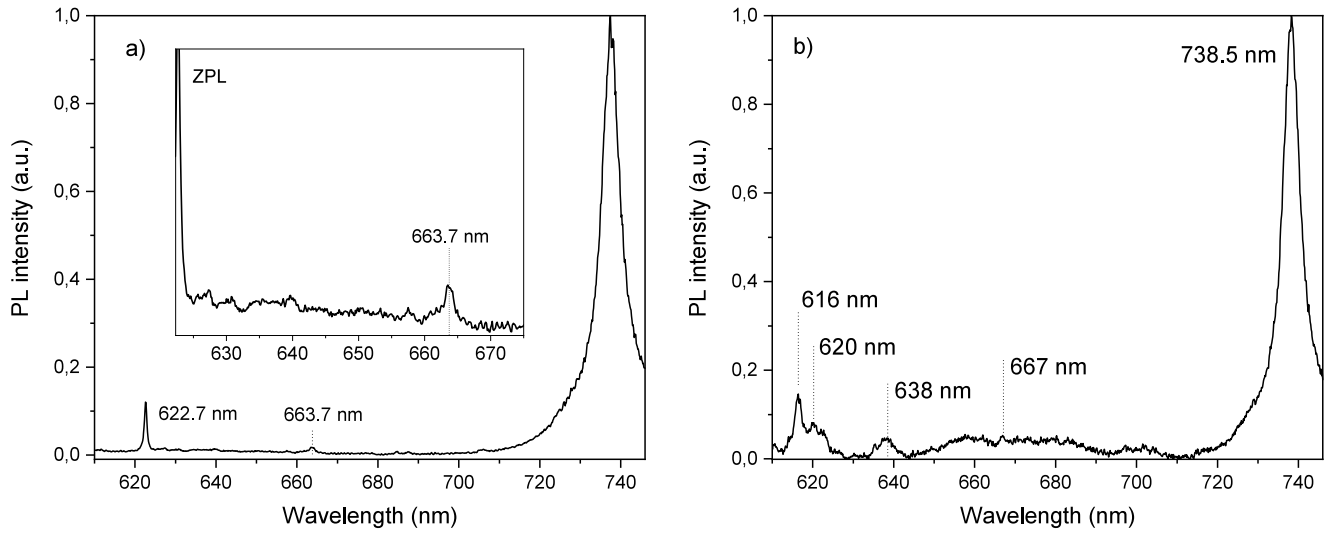

Figure 5. Room-temperature PL spectra of sample S750: (a) spectrum showing the 663 nm peak, and (b) spectrum exhibiting complex PL peak structures.

CVD system.[21] In addition to SiV, the NV center at 639 nm and peaks centered at about 620 and 631 nm are also identifiable in the PL spectrum. In our experiments, the spectral feature around 620 nm is observed only in the diamond samples deposited in the presence of the Sn dopant source and is comparable to the ZPL of SnV in CVD diamond reported in the literature.[10]

The 631 nm PL peak is reported as the quasi-local vibrations of the Sn atom in the diamond lattice.[25] We occasionally observe the 631 nm PL peak without an accompanying SnV ZPL, thereby suggesting different origins of the spectral line that are currently unknown, surface defect,[11] or a Sn-related defect.[15] The SnV center sideband is characterized by the presence of six spectral lines observed at about 634, 644.5, 656, 660, 669.5, and 681 nm.[26] Emission lines at 647 and 663 nm are also reported for the SnV center in diamond.[27] We do not identify the above-mentioned peaks, including the most dominant 660 nm/663 nm peaks, as they could be hindered by the intense sideband of the negatively charged NV center.

Similar to SiV and GeV centers, the SnV ZPL position changes with the isotopic constitution and is strain-dependent.[21,23] The ZPL changes due to Sn isotopes are relatively small.[28] Thus, the ZPL shift observed in our sample is likely due to a strain-associated environment of the SnV center resulting from the CVD conditions or the trapped Sn deposits within the overgrown CVD diamond layer; hence, variations in SnV ZPL position can be expected. Figure 4(b) shows the distribution of PL peaks in sample S850, with the most frequent PL peaks between 612 and 620 nm. Presently, only a few studies report the SnV ZPL shift in diamond,[29] while the optical properties of SnV centers in diamond under axial stress are currently unavailable in the literature. It is thus challenging to discern the stress response of the SnV ZPL and the range of SnV ZPL from the histogram in Figure 4(b). Furthermore, the SnV center creation in sample S850 is sparse with a high spatial nonuniformity.

The fabrication of SnV in diamond is particularly challenging, as Group IV elements have a larger atomic size and their incorporation into the diamond lattice can be limited. Second, the presence of lighter elements such as oxygen, nitrogen, and hydrogen, and the weaker bond energy of Sn−C relative to the C−C and C−H bonds, inhibits Sn incorporation in diamond.[12] In the following section, we report an improved SnV creation in diamond using a lower substrate temperature.

Figures 4(c) and 4(d) show a representative room temperature PL spectrum and the histogram of the observed PL peaks in the sample S750, respectively. Similar to the S850 sample, the ZPL of the SiV defect remains the most intense in the S750 sample. Interestingly, the S750 PL spectra have an increased SnV ZPL intensity relative to the S850 sample. The differences are evident when comparing the PL spectra of S850 (Figure 4(a)) and S750 (Figure 4(c)). Both spectra are normalized to the ZPL of the SiV defect in their respective samples. This observation supports that there is an increased SnV generation in CVD diamond at a lower substrate temperature of 750 °C.

We also observe an increased NV center ZPL intensity and its associated phonon sideband in the sample S750. In our experiments, the MW PE CVD system base pressure is around 5×10^{-3} mbar. Thus, nitrogen is expected to be present in the CVD growth plasma. Similar observations for enhanced NV center formation at 700 °C−760 °C CVD diamond growth temperature are reported.[30,31] There are also deviations from this observation − SnV ZPL with low intensity is occasionally observed in the S750 sample (Figure 5(a)). And, in the absence of the NV center sideband, the 663 nm PL peak can be identified. Another relevant observation from the PL analysis is an improved spatial uniformity of SnV creation in sample S750. PL spectra were recorded at multiple positions in a scan area of about 100 μm × 100 μm at five different positions on each sample. The resulting data were then used to generate the histograms in Figure 4. PL peaks around 620 nm were observed more frequently in S750 than in the S850 sample for a comparable PL scan area (Figure 4(b)). Hereby, we conclude that the S750 sample CVD conditions promote SnV creation in diamond. Additionally, due to the lower substrate temperature, features such as dislocations are observed on the S750 sample surface, suggesting nonideal diamond growth conditions (SI Figure S4). In contrast, the S850 deposited at a higher growth temperature is mostly devoid of such features. These results indicate the limitations of the process: a lower substrate temperature promotes SnV

https://doi.org/10.1021/acsmaterialslett.5c01218
ACS Materials Lett. XXXX, XXX, XXX−XXX

Table 1. Calculated ZPL Position at the HSE06 Level of Theory Using the Difference in Energy between the Valence Band Maximum (VBM) and e_g Kohn–Sham (KS) One-Electron Levels (ZPL_{GS}) and the Difference in Total Energy between the Ground State and the System with One Electron Moved from the VBM to the e_g State, after Which the Atomic Structure Was Allowed to Relax (i.e. the Adiabatic Excitation Energy) ($ZPL_{\Delta E}$)[a]

		ZPL shift (exptl)				
		SnV concentration			ZPL shift (calcd)	
		0.195% (nm)	0.100% (nm)	Dilute-limit (nm)	PBE (nm/GPa)	HSE06 (nm/GPa)
SnV^0	ZPL_{GS}	553.39	562.16	571.36	1.32	0.64
SnV^-	ZPL_{GS}	491.11	494.73	498.53	1.00	0.89
SnV^0	$ZPL_{\Delta E}$	599.62	603.04	606.63	1.15	1.36
SnV^-	$ZPL_{\Delta E}$	590.82	594.08	597.50	1.40	1.37

[a]The infinite dilute limit is calculated as a linear extrapolation from the given supercells. The size of the ZPL shift is given as obtained for the 0.1% SnV concentration supercell, for both PBE and HSE06 functionals. In the case of compressive/tensile strain, the ZPL is blue/red shifted.

creation in diamond with improved spatial uniformity, whereas SnV is sparsely fabricated at higher substrate temperatures. We also note that these crystallographic defects in the S750 may lead to additional and complex PL peak structures, as shown in Figure 5(b). Such PL features are interesting for future studies.

A set of density functional theory (DFT) calculations was performed to investigate the effect of hydrostatic strain on the SnV center in diamond. More details on the computational methods can be found in the SI. Using the PBE and HSE06 functionals, we calculated the ZPL position and shift due to hydrostatic strain for a defect concentration of 0.195% (4 × 4 × 4 supercell, or 1950 ppm) and 0.1% (5 × 5 × 5 supercell, or 1000 ppm). The neutral (SnV^0) and negative charge (SnV^-) states of SnV are considered, though both SnV^0 and SnV^- centers draw a significant amount of electrons from their environment, resulting in a negatively charged defect (spatial charge), as evident from the calculated Hirshfeld-I charges.[32,33] This spatial charge accumulation also contributes to the size of the SnV center, resulting in a size equivalent to 3.8 − 5 carbon atoms. Similar to the GeV center,[34] there is a significant supercell size dependence for both the SnV^0 and SnV^- centers. And, assuming a linear trend, as observed for GeV, the infinite dilute limit (a linear extrapolation to 0 ppm) was calculated for comparison with the experimental ppm-level concentration.

The calculated ZPL energy is slightly overestimated using the HSE06 functional, resulting in a lower wavelength than the experimentally observed value (Table 1). Our calculated value of 590.92 nm (2.099 eV) for the $ZPL_{\Delta E}$ energy of SnV^- using the 4 × 4 × 4 supercell is in very good agreement with the value of 587.6 nm (2.11 eV) presented by Gali and Thiering for the same supercell and functional, though they applied a C_{2h} symmetry to the defect to account for Jahn–Teller distortion. In the current work, we retained the D_{3d} symmetry, as (i) hydrostatic strain is expected to retain the symmetry (based on group-theory) and (ii) the effect of Jahn–Teller distortion is expected to be limited, not giving rise to a qualitative difference. Furthermore, their calculations also show that the incorporation of spin–orbit coupling lowers this energy by about 20 meV to 2.09 eV (593.23 nm).[35]

Despite the limitations regarding absolute ZPL positions, DFT can provide valuable insights into relative positioning and shifts. We note that extrapolation to the dilute limit moves the ZPL position in the right direction, putting it even closer to the experimental values. Further, the $ZPL_{\Delta E}$ values are closer to the experimental observation, as DFT is a ground-state theory, the position of empty states is poorly described. Using the energy difference of the ground state with the adiabatic excitation energy corresponds to a constrained 'ground state' calculation, which is better described by DFT. For both approaches, it is shown that the SnV^0 is located at a higher wavelength than the SnV^-, with the difference being a mere 9 nm for the more accurate $ZPL_{\Delta E}$ approach. This may make it hard to distinguish them solely based on the ZPL position. This might also suggest that the observed 631 nm line is associated with the SnV^0 defect, although further research is needed.

The ZPL shift was calculated using the PBE and HSE06 functionals, for both the 4 × 4 × 4 and 5 × 5 × 5 supercells, with the external pressure obtained by fitting the energy-volume data to the Rose-Vinet equation of state. For the SnV^0, the ZPL shift is about three times larger than previously reported for the GeV^0.[36] Similar to the GeV system, the ZPL is red-shifted in the case of tensile strain, while a compressive hydrostatic strain results in a blue-shift of the ZPL. Considering the more accurate $ZPL_{\Delta E}$ approach, the PBE and HSE06 results are comparable. More importantly, the shift of the SnV^0 and SnV^- is roughly (PBE) to almost exactly (HSE06) the same, with a shift of 1.37 nm/GPa for hydrostatic conditions. In a polycrystalline diamond sample, residual stress due to local defects and grain boundaries is expected, although the induced stress may be limited to only a few GPa. This would result in red and blue-shifted ZPL of a few nm. However, in the case of GeV^0, linear strain gave rise to much larger shifts,[34] which could explain the larger observed shifts in this study.

In summary, we report on SnV centers in NCD and free-standing (110)-oriented MCD discs fabricated using MW PE CVD with SnO_2 as a solid dopant source. Room-temperature PL confirmed SnV formation, though spatial nonuniformity was consistently observed. In addition to the 620 nm ZPL, peak shifts were detected, consistent with lattice imperfections and residual stress. Sn deposits on the substrate surface, originating from SnO_2 reduction in the hydrogen-rich plasma, partially inhibited diamond growth but a modified substrate holder helped mitigate this issue. Importantly, our results demonstrate that substrate temperature critically influences SnV creation: at 850 °C, SnV centers were sparse, whereas at 750 °C, we observed enhanced ZPL intensity and improved spatial uniformity, despite the presence of growth-related dislocations. Complementary DFT calculations under hydrostatic conditions predict a ZPL shift of ≈1.37 nm/GPa, supporting our experimental observation of strain-related peak shifts. Together, these findings establish temperature control as a decisive factor in the scalable in situ fabrication of SnV

https://doi.org/10.1021/acsmaterialslett.5c01218
ACS Materials Lett. XXXX, XXX, XXX–XXX

centers in diamond via MW PE CVD, paving the way for their integration into quantum photonic platforms.

■ ASSOCIATED CONTENT

Supporting Information

. The Supporting Information is available free of charge at https://pubs.acs.org/doi/10.1021/acsmaterialslett.5c01218.

Detailed experimental section, additional substrate details, substrate preparation methods, results of SEM, Raman, schematic of modified substrate holder, optical images, and computational details used for the modeling of the SnV center in diamond (PDF)

■ AUTHOR INFORMATION

Corresponding Authors

Rani Mary Joy − *Institute for Materials Research (IMO), Hasselt University, 3590 Diepenbeek, Belgium; IMOMEC, IMEC vzw, 3590 Diepenbeek, Belgium;* orcid.org/0000-0001-8741-4908; Email: rani.maryjoy@uhasselt.be

Ken Haenen − *Institute for Materials Research (IMO), Hasselt University, 3590 Diepenbeek, Belgium; IMOMEC, IMEC vzw, 3590 Diepenbeek, Belgium;* orcid.org/0000-0001-6711-7367; Email: ken.haenen@uhasselt.be

Authors

Miquel Cherta Garrido − *Photonics Research Group, INTEC-department, Ghent University-IMEC, 9052 Ghent, Belgium; Center for Nano- and Biophotonics (NB-Photonics), Ghent University, 9052 Ghent, Belgium*

Omar J. Y. Harb − *Photonics Research Group, INTEC-department, Ghent University-IMEC, 9052 Ghent, Belgium; Center for Nano- and Biophotonics (NB-Photonics), Ghent University, 9052 Ghent, Belgium*

Hendrik Jeuris − *Institute for Materials Research (IMO), Hasselt University, 3590 Diepenbeek, Belgium; IMOMEC, IMEC vzw, 3590 Diepenbeek, Belgium*

Rozita Rouzbahani − *Institute for Materials Research (IMO), Hasselt University, 3590 Diepenbeek, Belgium; IMOMEC, IMEC vzw, 3590 Diepenbeek, Belgium*

Jan D'Haen − *Institute for Materials Research (IMO), Hasselt University, 3590 Diepenbeek, Belgium; IMOMEC, IMEC vzw, 3590 Diepenbeek, Belgium;* orcid.org/0000-0003-4487-3885

Stephane Clemmen − *Photonics Research Group, INTEC-department, Ghent University-IMEC, 9052 Ghent, Belgium; Center for Nano- and Biophotonics (NB-Photonics), Ghent University, 9052 Ghent, Belgium; OPERA-Photonique CP 194/5 and Laboratoire d'Information Quantique CP 224, Université Libre de Bruxelles (ULB), 1050 Brussels, Belgium*

Dries Van Thourhout − *Photonics Research Group, INTEC-department, Ghent University-IMEC, 9052 Ghent, Belgium; Center for Nano- and Biophotonics (NB-Photonics), Ghent University, 9052 Ghent, Belgium;* orcid.org/0000-0003-0111-431X

Danny E. P. Vanpoucke − *IMOMEC, IMEC vzw, 3590 Diepenbeek, Belgium; Hasselt University, Institute for Materials Research (imo-imomec), Quantum & Artificial inTelligence design Of Materials (QuATOMs), 3500 Hasselt, Belgium;* orcid.org/0000-0001-5919-7336

Paulius Pobedinskas − *Institute for Materials Research (IMO), Hasselt University, 3590 Diepenbeek, Belgium; IMOMEC, IMEC vzw, 3590 Diepenbeek, Belgium;* orcid.org/0000-0001-8136-5172

Complete contact information is available at: https://pubs.acs.org/10.1021/acsmaterialslett.5c01218

Author Contributions

CRediT: **Rani Mary Joy** conceptualization, data curation, formal analysis, investigation, methodology, validation, visualization, writing - original draft, writing - review & editing; **Miquel Cherta Garrido** data curation, formal analysis, investigation, methodology, validation, visualization, writing - original draft, writing - review & editing; **Omar J.Y. Harb** data curation, formal analysis, investigation, methodology, validation, visualization, writing - original draft, writing - review & editing; **Hendrik Jeuris** data curation, investigation; **Rozita Rouzbahani** data curation, investigation; **Jan D'Haen** data curation, investigation, validation; **Stephane Clemmen** resources, supervision; **Dries Van Thourhout** resources, supervision; **Danny E. P. Vanpoucke** formal analysis, investigation, resources, software, writing - original draft, writing - review & editing; **Paulius Pobedinskas** supervision, writing - review & editing; **Ken Haenen** funding acquisition, project administration, resources, supervision, writing - review & editing.

Notes

The authors declare no competing financial interest.

■ ACKNOWLEDGMENTS

The authors acknowledge the funding from the Special Research Fund (BOF) via the Methusalem NANO network, and iBOF (BOF23IU12). The computational resources and services used in this work were provided by the VSC (Flemish Supercomputer Center), funded by the Research Foundation Flanders (FWO) and the Flemish Government − department WEWIS. S.C. is a research associate of the Fonds de la Recherche Scientifique (FNRS).

■ REFERENCES

(1) Nemoto, K.; Trupke, M.; Devitt, S. J.; Stephens, A. M.; Scharfenberger, B.; Buczak, K.; Nöbauer, T.; Everitt, M. S.; Schmiedmayer, J.; Munro, W. J. Photonic Architecture for Scalable Quantum Information Processing in Diamond. *Phys. Rev. X* **2014**, *4*, No. 031022.

(2) Ruf, M.; Wan, N. H.; Choi, H.; Englund, D.; Hanson, R. Quantum Networks Based on Color Centers in Diamond. *J. Appl. Phys.* **2021**, *130*, No. 070901.

(3) Golter, D. A.; Clark, G.; El Dandachi, T.; Krastanov, S.; Leenheer, A. J.; Wan, N. H.; Raniwala, H.; Zimmermann, M.; Dong, M.; Chen, K. C.; Li, L.; Eichenfield, M.; Gilbert, G.; Englund, D. Selective and Scalable Control of Spin Quantum Memories in a Photonic Circuit. *Nano Lett.* **2023**, *23*, 7852−7858.

(4) Osterkamp, C.; Mangold, M.; Lang, J.; Balasubramanian, P.; Teraji, T.; Naydenov, B.; Jelezko, F. Engineering Preferentially-Aligned Nitrogen-Vacancy Centre Ensembles in CVD Grown Diamond. *Sci. Rep* **2019**, *9*, 5786.

(5) Liu, K.; Zhang, S.; Ralchenko, V.; Qiao, P.; Zhao, J.; Shu, G.; Yang, L.; Han, J.; Dai, B.; Zhu, J. Tailoring of Typical Color Centers in Diamond for Photonics. *Adv. Mater.* **2021**, *33*, No. 2000891.

(6) Rodgers, L. V. H.; Hughes, L. B.; Xie, M.; Maurer, P. C.; Kolkowitz, S.; Bleszynski Jayich, A. C.; de Leon, N. P. Materials Challenges for Quantum Technologies Based on Color Centers in Diamond. *MRS Bull.* **2021**, *46*, 623−633.

(7) Iwasaki, T. Color Centers Based on Heavy Group-IV Elements. *Semiconductors and Semimetals* **2020**, *103*, 237−256.

(8) Chen, D.; Zheludev, N.; Gao, W. Building Blocks for Quantum Network Based on Group-IV Split-Vacancy Centers in Diamond. *Adv. Quantum Technol.* **2020**, *3*, No. 1900069.
(9) Bradac, C.; Gao, W.; Forneris, J.; Trusheim, M. E.; Aharonovich, I. Quantum Nanophotonics with Group IV Defects in Diamond. *Nat. Commun.* **2019**, *10*, 5625.
(10) Sedov, V.; Martyanov, A.; Neliubov, A.; Tiazhelov, I.; Savin, S.; Eremchev, I.; Eremchev, M.; Pavlenko, M.; Mandal, S.; Ralchenko, V.; Naumov, A. Narrowband Photoluminescence of Tin-Vacancy Colour Centres in Sn-Doped Chemical Vapour Deposition Diamond Microcrystals. *Philos. Trans. R. Soc. A* **2024**, *382*, No. 20230167.
(11) Iwasaki, T.; Miyamoto, Y.; Taniguchi, T.; Siyushev, P.; Metsch, M. H.; Jelezko, F.; Hatano, M. Tin-Vacancy Quantum Emitters in Diamond. *Phys. Rev. Lett.* **2017**, *119*, No. 253601.
(12) Ekimov, E. A.; Lyapin, S. G.; Kondrin, M. V. Tin-Vacancy Color Centers in Micro- and Polycrystalline Diamonds Synthesized at High Pressures. *Diam. Relat. Mater.* **2018**, *87*, 223−227.
(13) Palyanov, Y. N.; Kupriyanov, I. N.; Borzdov, Y. M. High-Pressure Synthesis and Characterization of Sn-Doped Single Crystal Diamond. *Carbon* **2019**, *143*, 769−775.
(14) Rugar, A. E.; Lu, H.; Dory, C.; Sun, S.; McQuade, P. J.; Shen, Z.-X.; Melosh, N. A.; Vučković, J. Generation of Tin-Vacancy Centers in Diamond via Shallow Ion Implantation and Subsequent Diamond Overgrowth. *Nano Lett.* **2020**, *20*, 1614−1619.
(15) Fujiwara, M.; Ohori, M.; So, F. T. K.; Makino, Y.; Morioka, N.; Ohki, I.; Igarashi, R.; Nishikawa, M.; Mizuochi, N. Single Tin-Vacancy Center in Nanoscale Diamond. *Discovery Nano.* **2025**, *20*, 81.
(16) Westerhausen, M. T.; Trycz, A. T.; Stewart, C.; Nonahal, M.; Regan, B.; Kianinia, M.; Aharonovich, I. Controlled Doping of GeV and SnV Color Centers in Diamond Using Chemical Vapor Deposition. *ACS Appl. Mater. Interfaces* **2020**, *12*, 29700−29705.
(17) Sedov, V. S.; Martyanov, A. K.; Altakhov, A. S.; Savin, S. S.; Dobretsova, E. A.; Tiazhelov, I. A.; Pasternak, D. G.; Kaplunov, I. A.; Rogalin, V. E.; Ralchenko, V. G. Formation of Germanium−Vacancy Color Centers in CVD Diamond. *J. Russ. Laser Res.* **2022**, *43*, 503−508.
(18) Bogdanov, K. V.; Baranov, M. A.; Feoktistov, N. A.; Kaliya, I. E.; Golubev, V. G.; Grudinkin, S. A.; Baranov, A. V. Duo Emission of CVD Nanodiamonds Doped by SiV and GeV Color Centers: Effects of Growth Conditions. *Materials* **2022**, *15*, 3589.
(19) Mary Joy, R.; Pobedinskas, P.; Baule, N.; Bai, S.; Jannis, D.; Gauquelin, N.; Pinault-Thaury, M.-A.; Jomard, F.; Sankaran, K. J.; Rouzbahani, R.; Lloret, F.; Desta, D.; D'Haen, J.; Verbeeck, J.; Becker, M. F.; Haenen, K. The Effect of Microstructure and Film Composition on the Mechanical Properties of Linear Antenna CVD Diamond Thin Films. *Acta Mater.* **2024**, *264*, No. 119548.
(20) Nguyen, T.; Sasaki, M.; Hsiao, S.; Tsutsumi, T.; Ishikawa, K.; Hori, M. Low-temperature Reduction of SnO_2 by Floating Wire-assisted Medium-pressure H_2 /Ar Plasma. *Plasma Processes Polym.* **2022**, *19*, No. 2100209.
(21) Bramble, J.; Moynihan, C.; Stemmley, S.; Stermer, J.; Robertson, J.; Weissburg, N.; Ruzic, D. N. Ejection of Molten Tin in the Presence of a Hydrogen Plasma. *Fusion Eng. Des.* **2024**, *207*, No. 114622.
(22) Mary Joy, R.; Pobedinskas, P.; Bourgeois, E.; Chakraborty, T.; Goerlitz, J.; Herrmann, D.; Noel, C.; Heupel, J.; Jannis, D.; Gauquelin, N.; D'Haen, J.; Verbeeck, J.; Popov, C.; Houssiau, L.; Becher, C.; Nesládek, M.; Haenen, K. Photoluminescence of Germanium-Vacancy Centers in Nanocrystalline Diamond Films: Implications for Quantum Sensing Applications. *ACS Appl. Nano Mater.* **2024**, *7*, 3873−3884.
(23) Nelz, R.; Görlitz, J.; Herrmann, D.; Slablab, A.; Challier, M.; Radtke, M.; Fischer, M.; Gsell, S.; Schreck, M.; Becher, C.; Neu, E. Toward Wafer-Scale Diamond Nano- and Quantum Technologies. *APL Mater.* **2019**, *7*, No. 011108.
(24) Lindner, S.; Bommer, A.; Muzha, A.; Krueger, A.; Gines, L.; Mandal, S.; Williams, O.; Londero, E.; Gali, A.; Becher, C. Strongly Inhomogeneous Distribution of Spectral Properties of Silicon-Vacancy Color Centers in Nanodiamonds. *New J. Phys.* **2018**, *20*, No. 115002.
(25) Chen, C.; Mei, Y.; Cui, J.; Li, X.; Jiang, M.; Lu, S.; Hu, X. Man-Made Synthesis of Ultrafine Photoluminescent Nanodiamonds Containing Less than Three Silicon-Vacancy Colour Centres. *Carbon* **2018**, *139*, 982−988.
(26) Tchernij, S. D.; Herzig, T.; Forneris, J.; Küpper, J.; Pezzagna, S.; Traina, P.; Moreva, E.; Degiovanni, I. P.; Brida, G.; Skukan, N.; Genovese, M.; Jakšić, M.; Meijer, J.; Olivero, P. Single-Photon-Emitting Optical Centers in Diamond Fabricated upon Sn Implantation. *ACS Photonics* **2017**, *4*, 2580−2586.
(27) Görlitz, J.; Herrmann, D.; Thiering, G.; Fuchs, P.; Gandil, M.; Iwasaki, T.; Taniguchi, T.; Kieschnick, M.; Meijer, J.; Hatano, M.; Gali, A.; Becher, C. Spectroscopic Investigations of Negatively Charged Tin-Vacancy Centres in Diamond. *New J. Phys.* **2020**, *22*, No. 013048.
(28) Corte, E.; Sachero, S.; Ditalia Tchernij, S.; Lühmann, T.; Pezzagna, S.; Traina, P.; Degiovanni, I.; Pietro; Moreva, E.; Olivero, P.; Meijer, J.; Genovese, M.; Forneris, J. Spectral Emission Dependence of Tin-Vacancy Centers in Diamond from Thermal Processing and Chemical Functionalization. *Adv. Photonics Res.* **2022**, *3*, No. 2100148.
(29) Narita, Y.; Wang, P.; Ikeda, K.; Oba, K.; Miyamoto, Y.; Taniguchi, T.; Onoda, S.; Hatano, M.; Iwasaki, T. Multiple Tin-Vacancy Centers in Diamond with Nearly Identical Photon Frequency and Linewidth. *Phys. Rev. Appl.* **2023**, *19*, No. 024061.
(30) Vindolet, B.; Adam, M.-P.; Toraille, L.; Chipaux, M.; Hilberer, A.; Dupuy, G.; Razinkovas, L.; Alkauskas, A.; Thiering, G.; Gali, A.; De Feudis, M.; Ngandeu Ngambou, M. W.; Achard, J.; Tallaire, A.; Schmidt, M.; Becher, C.; Roch, J.-F. Optical Properties of SiV and GeV Color Centers in Nanodiamonds under Hydrostatic Pressures up to 180 GPa. *Phys. Rev. B* **2022**, *106*, No. 214109.
(31) Tallaire, A.; Lesik, M.; Jacques, V.; Pezzagna, S.; Mille, V.; Brinza, O.; Meijer, J.; Abel, B.; Roch, J. F.; Gicquel, A.; Achard, J. Temperature Dependent Creation of Nitrogen-Vacancy Centers in Single Crystal CVD Diamond Layers. *Diam. Relat. Mater.* **2015**, *51*, 55−60.
(32) Prooth, J.; Petrov, M.; Shmakova, A.; Gulka, M.; Cigler, P.; D'Haen, J.; Boyen, H.; Nesladek, M. Long Spin Relaxation Times in CVD-Grown Nanodiamonds. *Adv. Quantum Technol.* **2023**, *6*, No. 2300004.
(33) Vanpoucke, D. E. P.; Bultinck, P.; Van Driessche, I. Extending Hirshfeld-I to Bulk and Periodic Materials. *J. Comput. Chem.* **2013**, *34*, 405−417.
(34) Vanpoucke, D. E. P.; Van Driessche, I.; Bultinck, P. Reply to 'comment on "Extending Hirshfeld-I to Bulk and Periodic Materials."'. *J. Comput. Chem.* **2013**, *34*, 422−427.
(35) van Wijk, T. G. I.; Melan, E. A.; Mary Joy, R.; Guillaume, E. Y.; Pobedinskas, P.; Haenen, K.; Vanpoucke, D. E. P. The Impact of Strain on the GeV-Color Center in Diamond. *Carbon* **2025**, *234*, No. 119928.
(36) Thiering, G.; Gali, A. Ab Initio Magneto-Optical Spectrum of Group-IV Vacancy Color Centers in Diamond. *Phys. Rev. X* **2018**, *8*, No. 021063.

https://doi.org/10.1021/acsmaterialslett.5c01218
ACS Materials Lett. XXXX, XXX, XXX−XXX